Performance Evaluation of LiDAR Point Clouds towards Automated FOD Detection on Airport Aprons

Johannes Mund[1], Alexander Zouhar[1], Lothar Meyer[2], Hartmut Fricke[2] and Carsten Rother[1]
Technische Universität Dresden
Dresden, Germany
[1]{johannes.mund, alexander.zouhar, carsten.rother}@tu-dresden.de
[2]{meyer, fricke}@ifl.tu-dresden.de

ABSTRACT
Both the current system of airport ground control and the continuous implementation efforts of A-SMGCS and Remote Tower concepts require complete and independent surveillance coverage in real-time. We believe that 3D point clouds generated by an actively scanning LiDAR system available at TU Dresden may satisfy these high standards. Nonetheless, the utilization of LiDAR sensing for airport ground surveillance purposes is extremely challenging due to the unique requirement profile in this domain. This is also the reason why existing solutions in other domains such as autonomous driving and robotics are not directly applicable for airport ground surveillance. In a first step, we developed point cloud object detection and segmentation techniques to present that new data comprehensively to the airport apron controller. In this paper, we focused on the timely detection of dislocated objects (foreign object debris, forgotten equipment etc.) as a serious cause to hazardous situations on airport movement areas. The results are promising for various reference targets. However, the detection of very small objects (e.g. socket wrench) requires more elaborate algorithms to take full advantage of the current LiDAR technology. In the future we will assess the strength of LiDAR-based surveillance in terms of the number of hazardous situations that could be avoided or safely managed by the apron controller.

Categories and Subject Descriptors
• Applied Computing~Physical sciences and engineering~Aerospace • Computing methodologies~ Computer vision~ Computer vision problems~Object detection

Keywords
LiDAR; laser scanning; point cloud; airport surveillance; apron control; apron management service; object detection; foreign object debris; FOD

1. INTRODUCTION
In our concept studies in [1] and [2] we clearly explained why airport ground operations, in particular those on the apron area, are regarded as significant risk drivers in the aviation sector. The apron, which can be characterized as an unstructured working environment with a large variety of objects, is a major contributor to this risk situation. Numerous activities of moving aircraft (AC), vehicles, equipment and personnel are additional factors that make the apron a complex and dynamic system [3] [4], causing even severe incidents and accidents [5] [6]. Except for the runway [7], the apron is to be considered as one of the most hazardous working environments at the airport.

At the same time, almost all stakeholders operating on the apron rely on the see-and-avoid principle, which in turn is primarily based on the direct view. Typical limitations of this principle are the sensitivity against view-restricting weather and lighting conditions, its dependency on the line-of-sight, and resolution limitations of the human eye. Even *looked-but-failed-to-see-errors* [8] can be potentially related to this principle. In addition to the direct view, also supporting ground radar (X and K_u-band) and video cameras are subject to physical limitations that do not allow for permanent and overall apron surveillance. An exemplary, yet important problem is the timely detection[1] of *foreign object debris* (FOD) on the airport`s surfaces, which could not be solved until today. The large number of conventional surveillance equipment deployed at today's airports demonstrates that other alternative systems (e.g. millimeter wave Radar (W-band) and infrared sensors) have not succeeded in establishing themselves.

Taking into account the apron`s characteristics and the limitations in the current surveillance capabilities, an information deficit resulting from a discrepancy between the information demand and the information available can be attested. As apron control is the overall authority to create and maintain operational safety, a reduced situational picture on the part of this operator most likely contributes significantly to the current risk situation on the apron. At the same time, this central role makes the apron control the most promising starting point for new approaches to risk mitigation (refer to [2]).

Here we derive our research`s objective, which is motivated by improving the safety level of apron operations beyond current targets, e.g. the ICAO *Advanced Surface Movement Guidance and Control Systems*-Concept`s (A-SMGCS) target level of safety [9]. To mitigate the risk of incidents and accidents our approach foresees to improve the situational picture of tomorrow's apron control through the provision of sensor data input that is new to the sector of airport ground surveillance.

To identify an appropriate sensing technology we performed a review on established sensors in other domains than aviation (refer to [2]). The review focused on domains that, firstly, call for automated object detection, -classification and -tracking and, secondly, that are established in unstructured and dynamic environments (e.g. autonomous driving, robotics, defense). Here, especially the domain of autonomous driving was found to fulfill these conditions to a large extent. We learned that this progress was significantly bolstered by the utilization of 3D point clouds generated through LiDAR sensing. LiDAR, which stands for *Light Detection and Ranging*, is a non-cooperative Laser beam-based method to measure distances between the sensor and any reflecting object.

We would like to thank the DFG (German Research Foundation) most sincerely for funding the research presented in this paper (FR 2440/4-1).

1 According to Johnson [45] detection is about perceiving the "presence of an object".

The capabilities of LiDAR-based real-time perception in operation were successfully demonstrated in the *DARPA Urban Challenge* (2007) and the *Civilian European Land Robot Trial* (2007) [10]. At both events conventional vehicles had been equipped with a *Velodyne HDL-64E* LiDAR - a sensor that is characterized by its 360° horizontal field-of-view (FOV) and its capability to provide 3D point data in real-time. In the research project "Stadpilot" a *Volkswagen Passat*, which had been equipped with LiDAR and radar sensors, became one of the first vehicles to drive autonomously on real city roads with real traffic (e.g. described in [11]).

To summarize, LiDAR combined with other sensors like video, infrared and/or radar have become a backbone for research and operationalization in the field of autonomous driving. Comparability of the autonomous driving domain with airport surface operations exists, as explained earlier. Despite these similarities, the scope of research and development of these two domains is much different. In autonomous driving, the main focus is on methods that process point cloud data along with multiple other sensor inputs, with the objective, to provide these data in a converted, machine-readable format to an automat acting as an end user (e.g. target tracking at robot cars [12], sensor fusion in [13]). In the context of aviation, real-time data processing is a major challenge, too. However, we also have to spend considerable efforts on the way the point data may be presented to a human operator[2]. This in turn requires taking existent ATM regulations and procedures as well as current surveillance concepts and deployed technologies related to apron surface surveillance into account. Another difference to the autonomous driving domain: A safety-effective apron surveillance capability will require a detection and classification functionality for even very small objects in a significantly larger coverage area.

For the reasons given about, we chose LiDAR-generated sets of three dimensional (3D) data points (so called point clouds) to be provided at the apron controller working position (CWP). LiDAR sensing is characterized by its wavelength spectrum from ultraviolet to near-infrared (≈400nm to ≈3000nm) and the resulting extraordinarily high frequencies reaching into petahertz range[3]. For comparison purposes: Common primary radar uses lower frequencies in the gigahertz range. As a result, radar has a longer range than LiDAR, but suffers from target-splitting effects, poor coverage and low resolution [14] [15] [16].

The following description therefore summarizes the expected advantages of LiDAR sensing over other established airport surveillance technologies, in particular video camera, primary surveillance radar (PSR), secondary surveillance radar (SSR) and multi-lateration systems (MLAT). The advantages listed below arise from both the properties of the laser beam and construction-related factors of the sensor:

- A non-cooperative measurement principle ensuring independence from a target`s active response signal (compared to SSR, MLAT etc.): As such, even non-cooperative objects (e.g. FOD or apron personnel) can be detected. Furthermore, this concept is compliant to the SESAR Air Traffic Management (ATM) Target Concept D3 [17], which calls for the utilization of non-cooperative sensors to enhance the operator`s situational picture.
- Capability to derive the depth "z" of an object: This considerably supports the extraction progress of 3D objects from the data [18]. Video cameras or infrared cannot generate information about scene depth, whereas PSR only measures the slant range.
- High pulse repetition rate (PRR) and high pulse intensities result in good temporal and spatial resolution compared to common PSR, and even high-resolution millimeter wave radar: This is most beneficial for the extraction of geometric features from raw data [19], e.g. spatial dimensions, positions.
- Reduced sensitivity against adverse visual conditions compared to the human eye and standard video camera [20].

The above characteristics will help to technically realize our research approach: To develop and implement a point cloud-based surveillance concept that is capable to recognize (emerging) hazardous situations by their typical patterns (pattern recognition). Supported by post-processed point cloud data visualized on an additional screen to the controller, he should be enabled to take corrective actions in time to avoid or manage hazardous situations. Figure 1 depicts the proposed surveillance concept along with a default apron CWP. The fusion of 3D point data with sensor input from the existing means of surveillance (radar, video) will be considered at a later stage of the research (for details refer to [2]).

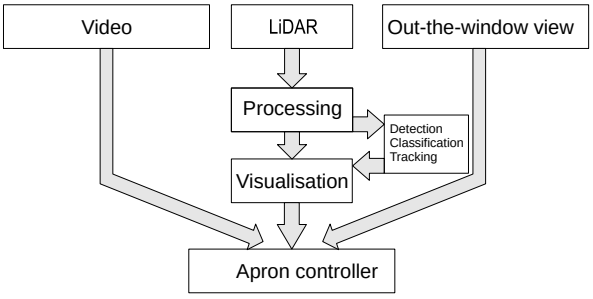

Figure 1. Components and key functions of the point cloud-based surveillance concept for apron control

It is well understood that the described pattern recognition builds on the core capability to effectively and reliably detecting physical objects. By proposing a LiDAR point-based object detection technique and by demonstrating its technical feasibility in this paper, we not only create a solid basis for higher-level functions, but also contribute to the yet unsolved issue of detecting dislocated objects on airport surfaces, better known as FOD.

In section 2, the methodological framework for the underlying risk mitigation approach, essentially a risk assessment (RA), is briefly explained, using Dresden airport (DRS) as a reference example. This will be followed by a discussion on the specific need for detecting physical objects, and in particular FOD, on airport surfaces. In a two-step approach, section 3 provides insight into object detection by LiDAR 3D points both on an algorithmic and a physical-technical level. In the following subsections, metrics for evaluating object detection performance will be derived. In preparation of a field trial to determine *detectability* and *time to detection* using LiDAR-technology, an experimental design is set up in section 4. Whereas section 5 presents the respective results, section 6 will discuss them in terms of potential contributions for safer apron operations in ATM.

[2] TU Dresden is currently developing concepts for a point cloud-based visual human-machine interface for the apron control unit carried out with the chair of Engineering Psychology and Applied Cognition and apron controllers from Dresden airport.

3 The sensor available at TU Dresden (OPAL 360 series) uses a wavelength of 1540nm.

2. BACKGROUND

In section 1, we explained our motivation to increase the safety level of apron operations. In this section, the methodological background to the underlying risk mitigation approach will be laid down briefly. In this regard, an overview on our currently ongoing risk assessment (RA) will be provided. The RA shall deliver functional requirements for a safety-effective provision of LiDAR point cloud data to the apron controller. The functionality of object detection will be put into this context, and will then be further explained on the example of detecting FOD.

2.1 Overarching Risk Assessment

In our concept study [2] we identified a discrepancy between the operator´s *information demand* and the *information provision* available at the CWP as a main reason for the current risk situation on aprons. Our risk mitigation approach foresees to fight the resulting *information deficit* by providing point cloud data to the apron controller. This new information shall be presented on an additional screen at the CWP. The development of such a "socio-technical system" (e.g. defined by *Hollnagel* [21]) normally follows functional- and non-functional requirements[4]. The group of functional requirements will be considered as concrete countermeasures to the identified *information deficit*, determining quality, quantity, and time of provision of point cloud data at the CWP. The overall causal relationship is depicted in Figure 2:

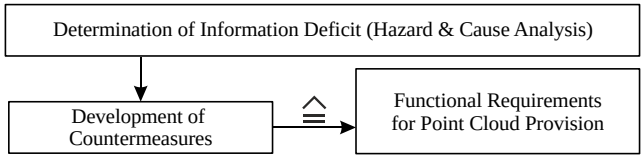

Figure 2. Causal chain for deriving functional requirements

The definite determination of the *information deficit* is crucially important for the success of the approach. To do so, we performed a hazard and cause analysis as part of a RA[5]. This involved the analysis of all surveillance related tasks and processes of the apron control at Dresden airport (including the *information demand*), as well as the collection of all information sources available at the CWP (*information provision*). To gain insights about the information deficit, hazards that can be attributed to an unbalanced relation between information provision and demand were identified, followed by the determination of possible consequences and probable causes. We defined a hazard as follows:

"An insufficient information acquisition on the part of the controller in a specific situation demanding for specific information to safely execute the control and surveillance task of the apron control"

Two main failure modes with a potentially negative impact on the controller`s situational picture were specified:

- total or partial absence of demanded information
- cognition of defective information

The failure modes were considered within multiple brainstorming sessions with experts from Dresden airport (apron controllers, airport safety manager) to build the hazard list. Even hazards from completed safety assessments were reviewed and added to the list if and where appropriate (e.g. a subproject to *innovativer Flughafen*, iPort [22]). Upon completion, the list contains 44 hazards.

As the detection functionality is in the scope of this paper, we analyzed the individual hazards regarding their potential relationship to the presence of physical objects. The following initial observation was made: 35 of 44 hazards (≈80%) are substantially related to the presence of at least one physical object / solid target (e.g. A/C, ground vehicle, FOD, guidance lines etc.). As such, we have an indication about the importance of a fully functional detection capability for solid targets. This finding is independent from to be developed specific measures to fight each of the identified hazards (not discussed in this paper). The effectiveness of our risk mitigation approach will be evaluated at a later stage of our research. This will involve human-in-the-loop simulations with real apron controllers and a limited in-the-field validation at Dresden airport.

2.2 Risk of Undetected FOD

In the scope of the ongoing RA, we will investigate the capability of the proposed LiDAR system to address an exemplary, but nevertheless important hazard. We identified the undetected presence of dislocated objects on airport surfaces as serious, empirically proven safety issue for the ATM domain that has not yet been solved satisfactorily. Consequently, the resulting hazard can be found in our hazard list (refer to section 2.1), namely: "Physical Presence of FOD not perceived".

The Federal Aviation Administration (FAA) defines FOD as [23] *"Any object, live or not, located in an inappropriate location in the airport environment that has the capacity to injure airport or air carrier personnel and damage aircraft"*. According to Eurocontrol [24], the physical features of FOD are of typical dimensions equal to or less than approx. 6 cm2 and dark colour in more than 50% of all cases.

Multiple FOD-related incidents and accidents show that both severity and probability of occurrence of FOD events are eminent enough to pose a significant risk for airport surface operations worldwide. The best known example of an FOD accident is the Concorde crash in 2000 near Paris, France with 113 casualties [25]. An Australian statistic [5] points out that five of 41 recorded ground occurrences at airports in Australia could be attributed to FOD. According to the National Aerospace FOD Prevention, Inc. [26] damage by FOD causes US$4 billion a year. The consulting group Insight SRI states that even this amount could be undervalued [27]. In addition SRI analyzed that 207 of 287 incidents per million flight operations occur due to the presence of FOD on the runway.

Apart from the preferred solution to prevent the presence of FOD at all, the need to quickly and reliably detect FOD once they occurred is set forth by ICAO [28]: "*The surfaces of all movement areas including pavement shall be inspected […] with the objective of avoiding and eliminating any loose objects/debris that might cause damage to aircraft or impair the operation of aircraft systems."* However, the few existing FOD detection systems, e.g. the *QinetiQ's Tarsier system* [29], are exclusively designed for runway inspections, and have been deployed rarely to airports so far. By proposing FOD detection from a single LiDAR source as one of many issues that are dealt with in our ongoing RA, we take a new technological approach to address this relevant safety issue.

[4] Non-functional requirements are often further differentiated into qualitative (safety requirements, ergonomic requirements etc.) and quantitative requirements (e.g. performance requirements etc.).

[5] The Functional Hazard Assessment (FHA) of Eurocontrol Safety Assessment Methodology (SAM) [46] served as a methodical framework.

2.3 Risk Contribution of Controller`s Inadequate Situational Awareness

As explained in section 1, we see the apron controller as most promising starting point for risk mitigation, assuming that the post-processed point cloud data will enhance his situational awareness. An (apron) controller`s activities are generally based on two main factors: Task definition and situational awareness. The first component is fixed by the manual operations, whereas the latter is the actual intended addressee in our approach.

Endsley [30] defines situational awareness as *"perception of the elements in the environment within a volume of time and space, the comprehension of their meaning and the projection of their status in the near future"*. By visually forwarding information on detected objects to an human operator, the first level of Endsley`s model of situation awareness [31] is addressed: Perceiving *"[...] the status, attributes, and dynamics of relevant elements in the environment*" (see Figure 3).

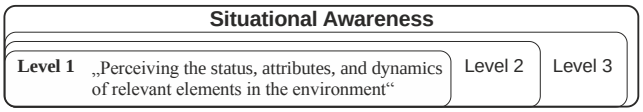

Figure 3. Endsley`s model of situational awareness [31]

This is why, level 1 is essential for generating the controller`s situational picture. This level has a high impact on safety, as missing or incorrect information can potentially result in a reduced surveillance capability or, even worse, in wrong decisions. Niessen and Eyferth [4], who adopted Endsley`s model to the ATC domain, consequently assigned level 1 to the *monitoring cycle* (building up the controller`s mental image and keeping it up to date).

Jones and Endsley [32] analyzed the *Aviation Safety Reporting System* (ASRS) in terms of potential failures in the controller`s situational awareness and proofed level 1 as most important in terms of situational awareness: 72.4% of all safety-critical events that occurred in the aviation sector were found to be level 1 failures („Fail to perceive information or misperception of information"), whereas 20% of these events could be attributed to level 2 ("Comprehension of current situation") and 4% to level 3 failures ("Projection of future states").

Regarding these numbers, our approach to improve the controller`s level 1 situational awareness by providing an independent detection functionality is confirmed[6].

3. DETECTION METHODOLOGY

In accordance to the findings of section 2, we aim at demonstrating technical feasibility of LiDAR point cloud-based ground surveillance for detecting physical objects, in particular FOD, on the apron. This section gives an insight into object detection from LiDAR data on an algorithmic level, followed by short background information regarding physical and technical aspects of 3D point generation at signal level. In preparation of the field trial in section 4, we will also derive metrics for evaluating the object detection performance of the proposed LiDAR system.

[6] At a later stage, it is foreseen to bolster Endsley`s [42] level 2 and level 3 situational awareness. However, as both level 2 and 3 go far beyond the detection of objects, they are not considered any further in this paper.

3.1 Techniques for Object Detection

In this section we explain our approach to detecting and segmenting objects in LiDAR-based 3D point cloud scans. The traditional problem addressed by object detection and segmentation is to find objects of known types in images and to separate them from the background. State of the art methods in computer vision often cast such tasks as labeling problem where we are given an image and need to predict labels.

In this work we focus on the detection and segmentation of static objects in 3D point clouds where we assume that the objects of interest tend to be small compared to the rest of the scene. This complies with a typical FOD scenario where small dislocated objects can cause hazardous situations. Given a 3D point cloud scan of an apron scene the task is to assign each point a label (class membership), i.e., either foreground (fg) or background (bg).

The task poses at least three challenges. Firstly, a typical apron scene is a highly congested environment with many different types of objects (e.g. FOD, vehicles, aircraft) and where bg-structures act as distractors. Secondly, objects can be occluded or may constitute so called "unseen-before object types". From this it follows that the notion of what constitutes an object must be general enough in order to yield segmentations of sufficient quality. Thirdly, we do not have labeled objects at our disposal. This poses a limitation on the set of available methods suitable for this task.

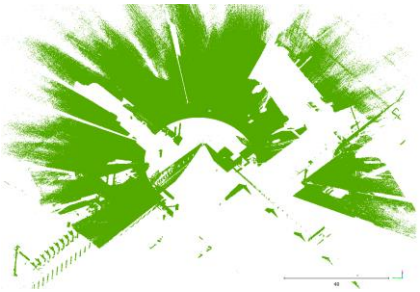

Figure 4. Example 3D point cloud scan representing an apron field

In the present task we are given time stamped position data in 3D Cartesian format (x, y, z) where the point clouds to be processed tend to be dense and large. A typical apron scan, for example, contains about 40 million points (see Figure 4). Moreover, we have a baseline 3D scan of an apron scene at our disposal. Such a scan contains surfaces which we assume to be fixed static elements of the scene (e.g., buildings, light poles).

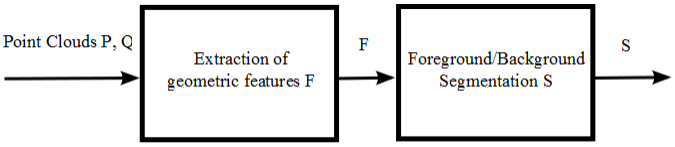

Figure 5. Overview of the detection and segmentation schema

Figure 5 depicts our proposed detection and segmentation schema. The algorithm takes as input a 3D point cloud P representing an apron scene (Figure 4) together with a bg scan Q and creates as output a segmentation and labeling S (Figure 7), where each point $p \in P$ is associated with a segment, and every segment has a label (fg/bg). In order to validate the performance of the algorithm the target point cloud P contains six test objects which were placed on the apron field prior to scanning, namely the objects A through F (refer to section 4 for a detailed description). We now describe the two steps in detail.

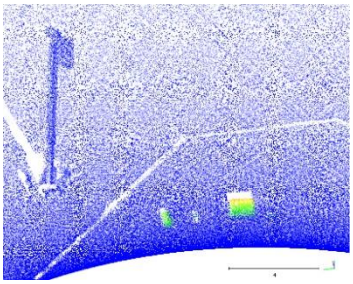

Figure 6. Distance mapping: Shown is the section of *P* where the test objects A-F are located. The color mapping encodes the Euclidian distance of each point in *P* to the closest point in the baseline scan *Q* ranging from small (blue) to large distances (red). Larger distances indicate potential object candidates.

Since objects inserted in the scene are likely to rise above their surroundings a reasonable approach to finding object candidates in *P* is to compute the Euclidian distance of a point $p \in P$ to the closest point q in the baseline scan Q.

To cope with the large amount of data we use occupancy grids known from robotic mapping to identify object candidates (see e.g. [33]) and k-d trees for fast nearest neighbor searches. On a standard PC the runtime for the extraction of geometric features (first block in Figure 5) amounts to 30s where $|Q| \sim 90$ million and $|P| \sim 40$ million.

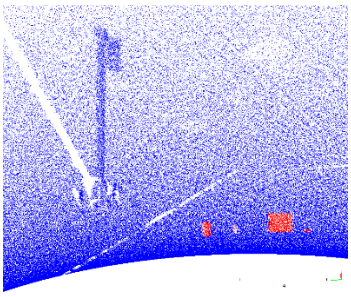

Figure 7. Foreground-background segmentation of the target point cloud *P* where red denotes foreground and blue denotes background. From left to right the detected and segmented objects are: A, B, D, E.

The fg-bg segmentation task may be formulated in terms of energy minimization. Let $L = \{0,1\}$ denote a set of labels where 0 means bg and 1 means fg. Moreover we define the Euclidian distance of a point $p_i \in P, i \leq |P|$ from the closest baseline point $q \in Q$ as local feature $f_i \geq 0$. The task is to find a labeling $S: P \rightarrow L$ which assigns every point $p_i \in P$ a label $s_i \in L$ by relating the observed features F to the labels in a spatially coherent way, i.e., the labels f_i, f_j of nearby points $p_i, p_j \in P$ are more likely to agree. The formal task is then to find a labeling *S* that minimizes an energy function E(S), i.e.,

$$E(S) = \sum_i \lambda_1 f_i + \sum_i x_i(1 - f_i) + \cdots$$

$$\ldots + \sum_{ij \in N_i} w_{ij} \delta(f_i, f_j) \rightarrow \min_S, \qquad (1)$$

where $w_{ij} = \lambda_2 / ||p_i - p_j||_2$, $\delta(s_i, s_j)$ denotes the Kronecker-delta function and N_i contains the k −nearest neighbors of p_i in *P* where the parameters $\lambda_1, \lambda_2 \geq 0$ need to be estimated from training data. In our experiments we found $k = 10, \lambda_1 = 0.05, \lambda_2 = 0.005$ to be a reasonable setting. Note, that equation (1) affords a global solution using graph-cuts for which we employ the method in [34]. In Figure 7 we show a zoomed in view of the section in P where the test objects are located. On a standard PC the fg-bg segmentation (second block in Figure 5) runs about 40s so that the total run time amounts to approx. 70s. In the above example point cloud *P*, our current algorithm was able to find 4 of 6 test objects, namely the objects A, B, D, E (refer to section 5 for a detailed description).

3.2 Performance Metric from Signal Theory

The fundamental basis for the application of the above algorithm (see section 3.1) is the availability of a minimum number of 3D points of each target object, so that detection/segmentation can be realized. On a physical-technical level a 3D "echo" is generated when a signal pulse sent out by the sensor is sufficiently reflected at a target`s surface, and then transmitted back with a certain reception power P_R above a predefined threshold. When adapting the LiDAR equations from *Wandinger* [35] and *Measures* [36] to the detection of solid targets using a monostatic LiDAR[7] and assuming the effective target area to be orthogonal to the laser beam, the following model equation for calculating $P_{R\_hard\ target}$ as a function of the laser`s wavelength λ and the distance x between sensor and target give rise to:

$$P_{R\_hard\ target}(x, \lambda) = P_0 \times \left(\frac{c\Delta t}{2}\right) \times A_R \times \ldots$$

$$\ldots \times \mu \times \frac{\rho}{\pi x^2} \times \exp(-2 \int_0^x \alpha(r, \lambda)) dr \qquad (2)$$

From this equation the following can be concluded: $P_{R\_hard\ target}$ is internally affected by the sensor parameters transmission power P_0, the size A_R of the receiver optics, the pulse length represented by $c\Delta t$, and the sensor specific efficiency factor μ. External factors on $P_{R\_hard\ target}$ are: The target reflection coefficient ρ[8], and the atmospheric transmission represented by the term $\exp(-2 \int_0^x \alpha(r, \lambda)) dr$, where $\alpha(r, \lambda))$ is the extinction coefficient[9].

From equation (2) we may draw the conclusion that the quantity $P_{R\_hard\ target}$ mainly depends on the distance x between the sensor and a hard target. This assumption is based on the inverse proportionality between $P_{R\_hard\ target}$ and the squared distance x. Reducing $P_{R_{hard}target}$ also means reducing the probability of receiving a reflection signal, which, as a result, cannot serve as input for the detection/segmentation algorithm.

On the basis of these conclusions, we will regard object *detectability over distance x* as a meaningful metric to evaluate the technical feasibility of the proposed LiDAR system for point-based object detection.

---

[7] The Laser emitter and receiver parts form one constructional unit (e.g. *Neptec OPAL series*)

[8] Influenced by angle of incident, surface material, laser wave length

[9] A measure for the attenuation of an electromagnetic wave passing through a medium, caused by absorption and scattering

3.3 Performance Metric from the Risk Mitigation Perspective

In the scope of the ongoing RA, we introduced the hazard "Physical Presence of FOD not perceived" as a relevant candidate to be addressed by the proposed LiDAR system (see section 2).

Accidents like the Concorde crash in 2000 emphasize the need for a quick detection of FOD. In this example, a small titanium strip was lost by another aircraft and indirectly caused the Concord to crash five minutes later [25]. Even though this worst case FOD accident took place on the runway, it is reasonable to transfer the overall context to apron operations. For instance, an FOD that is injected by a jet engine during taxiing on the apron might lead to an engine failure in a more critical phase. As any specifications/recommendations regarding minimum detection times for specific FOD types were not yet defined, the rule of thumb shall be "the sooner, the better". The currently ongoing RA (section 2.1) will deliver precise requirements regarding minimum detection times for various objects.

For the reasons given about, we introduce a second metric relevant for detecting objects, and especially FOD, namely the required *Time to Detection* (TTD) per object. We define TTD as the time span between the physical appearance of an object and its detection by the respective algorithm. Additional times for visualizing the data on a screen at the CWP, and times for perceiving and interpreting this information by the human operator are excluded from this definition.

With our system, the TTD is composed of two parts: The time available for acquiring reflection points (*acquisition time*) and the *computing times* of the object detection/segmentation algorithm. While the latter will become comparably low with continuing development in foreseeable future (target time: <5s), we assume that the data *acquisition time* will define the time critical path. The reason for this is based on the non-overlapping scan pattern of the LiDAR sensor available at TU Dresden (*OPAL 360 series)*. This scan pattern results from one single 1540nm pulsed class 1 laser beam passing two randomly rotating prisms. Due to the random rotation (each prism at 30 revolutions/s), a constant sensor FOV and 200000 pulses sent out each second, a single reflected pulse can be assumed to be uniformly distributed in the scanning area. The non-overlapping scan pattern is most valuable for stationary applications in dynamic surroundings (like our fixed-based installation at the airport), as gaps within the scanning range will theoretically close over time according to random theories.

In summary, the longer the *acquisition time*, the more the point density will increase. For detecting and segmenting any object located in any position in the sensor`s FOV, a certain critical point density will be required as an input for the detection/segmentation algorithm. For the reasons given about, the TDD will be analyzed in terms of its *acquisition time* component only, intentionally excluding the rather low *computing time* component from the analyses in this paper.

By using *detectability over distance* and TDD as metrics in our field trial, we expect to obtain important findings on what the combination of LiDAR and algorithms is capable in terms of a minimum detection performance. Those findings will be taken into account when developing point cloud-based countermeasures against an information deficit at the CWP within our ongoing RA (section 2.1).

4. EXPERIMENTAL DESIGN

4.1 Methods of Analysis

Based on the findings of section 3, a field trial will study the following dependent variables over various distances between the sensor and different target objects: *Detectability* and *Time to Detection* (TTD). The detectability measurements shall deliver universal statements on the combined performance[10] of both the sensor and the algorithm to detect different static objects. The target objects are divided into *standardized objects* and *real objects*. The use of standardized objects will allow us to keep target-related influential factors of equation (2) constant (see subsection 4.3 for details). In a subsequent step, the TTD to each successful detection shall be calculated. Here, the main goal is to derive a reference graph of detection times for the standardized objects as a function of distance. Further, the detection times of real objects (e.g. FOD) shall be compared with the reference graph.

4.2 Experimental Environment

A part of the apron of Dresden airport served as experimental environment. The different object positions were determined depending on the systematic variation of the distances between the sensor and the target objects. Prior to the field trial, the LiDAR sensor had been mounted on the terminal building`s roof in a total height of approx. 15m (see Figure 8). To gain the greatest possible coverage regarding relevant ground activities and to reduce shadowing, an analytical-geometric model developed at TU Dresden [37] was taken into consideration when selecting a suitable sensor position.

Figure 8. LiDAR sensor mounted at Dresden airport

The LiDAR sensor available at TU Dresden (*Neptec OPAL 360HP*) is capable to measure and output 3D reflection points in real-time. A 3D point represents a geo-referenced Cartesian coordinate (x,y,z) of the actual reflection point on a target. The percentage return-beam power ratio of every received signal is also stored. The maximum PRR amounts up to 200 kHz. For maximum range measurements, the number of pulses is limited to 25000 (25 kHz). The horizontal and the vertical FOV are 360° and 45°, respectively [38].

4.3 Experimental Configuration

The distance x between the sensor and the targets served as independent variable in our test series. Six distance steps (25 m, 60m, 95m, 130m, 165m, 200m) were defined according to the sensor`s technical range spectrum. This region of interest is, firstly, surrounded by a circular blind area of approx. 22 m (radius) in function of the vertical FOV and the mounting height, and secondly, limited by the chosen scan mode (Short Range: 200kHz PRR), where 200m represents the maximum range.

Object A, which is a member of the *standardized objects*, is standardized and idealized in terms of:

[10] The evaluation of the individual performances of sensor and algorithms is not the subject of this report.

- Size of the effective reflecting surface: 1 m2. Given that the laser footprint[11] is smaller than the target object, the size of the reflecting surface is neglectable from the single signal pulse perspective[12], and is therefore not included in equation (2). However, we assume that the number of captured 3D points per object increases with the size of the reflecting surface, giving rise to better detection performance of the algorithm.

- Reflectivity coefficient ρ: We used a retroreflector to gain a high reflectivity ($\rho \rightarrow 1$) by ensuring that the beam angle of incidents equals the angle of reflection (in accordance with the assumption of section 3.2: effective target area is orthogonal to the laser beam). As a supporting measure, we manually adjusted the angle between the target surface and the laser beam for each distant step. The background to this is that we wanted to ensure a constant, orthogonal vertical angle of incidence between sensor and the targets.

A standardized target like object A will allow us to draw conclusions on the detectability over distance, keeping the other main target-related influential factors of equation (2) constant (principle of Ceteris paribus). At the same time, a reference graph of TTD as a function of the distance may be plotted. With regard to the idealized characteristics of a standard object, the TTD graph and its behavior may be utilized to compare the overall detection performance of the LiDAR system with the direct view and other means of surveillance (e.g. primary Radar).

The primary *standardized object* (object A) was then extended by two other targets. Apart from the modified size of the effective reflecting surface, 0.063 m2 for object B and 6 cm2 for object C, all other standardization features were held fix. Whereas object B is one-sixteenth of the size of object A, the size of object C was intentionally defined as 0.0006 m2. The reason for this is that, according to Eurocontrol, typical FOD are of average dimensions equal to or less than approx. 6 cm2 [24]. With object C this dimension is represented in our study.

The group of the *real objects* contains objects that potentially may turn into FOD if (dis-)located on the apron`s surface. This group consists of a suitcase (object D), a toolbox (object E) and a wrench (object F). Just as for the *standardized objects*, the detectability and the TDD for the *real objects* shall be determined, so that the respective results of both groups become comparable. All objects used in our field study can be seen in Figure 9:

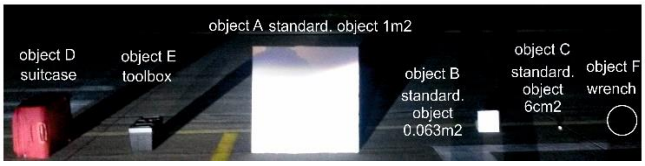

Figure 9. Reference and real objects used in the test series

In contrast to the *standardized objects*, the objects within the group of *real objects* were systematically rotated to prevent that one object orientation may distort the results. Whereas Pose 1 represents the smallest possible reflecting surface orthogonal to the laser beam (see Figure 9), pose 2 shall ensure the largest possible target surface within the sensor`s FOV by rotating the object 45° from pose 1.

In view of the parameters of equation (2), the following experimental conditions were created or were present:

- All sensor parameters were held constant during the field trials.
- All objects were placed in the line-of-sight, as the laser beam emission at 1540nm does not allow to take advantage of any diffraction effects and others.
- Atmospheric transmission: the view was clear without precipitation during the entire period.
- The apron surface was dry.

5. RESULTS

5.1 Qualitative Analysis

Prior to applying our detection and segmentation algorithm, we manually analyzed the captured raw data using a 3D viewer (e.g. *CloudCompare*). The screenshot in Figure 10 depicts a top-down view of a single service lane for ground vehicles alongside the apron. The color map in Figure 10 visualizes the height over ground along the z-axis of the scanner coordinate system. From the figure one can see that even extremely small structures (0.5mm to 2mm) are highlighted (e.g. road markings).

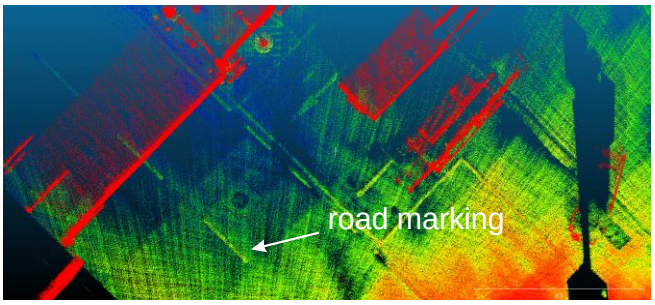

Figure 10. Height over ground visualization of an apron service lane at Dresden airport using a color map

Moreover, we identified physical effects in the data which we belief are related to the sensor`s measurement principle: In particular the reflectivity of the target surface and the corresponding beam angle of incident (both represented by the reflection coefficient in equation (2)) seem to be of high relevance for identifying object contours in the data. Referring to Figure 10, the material of the road markings has reflection properties which greatly benefit their distinction from the surrounding concrete surfaces. Interestingly, the reflection coefficient for concrete seems to be constant over the beam angle of incident. Puddles on the concrete were an exception: Here, the number of captured points decreases significantly. This may be explained by a modified, rather adverse angle of reflection, caused by the specific reflection properties of the water.

5.2 Detectability

In this section we validate the combined performance of the LiDAR sensor and the detection/segmentation algorithm. Unlike originally planned, it was not possible to carry out measurements at a distance of 135m due to ongoing aircraft operations. For each distance and pose the sensor runtime was about 8min (data acquisition time SAT_{total}) and resulted in approx. 42 million captured reflection points ($\#points_{total}$). After that, each data set was

[11] Area illuminated by the laser beam. Depends on beam divergence and laser optic`s FOV

[12] This is the case in our field study, as both the sensor`s laser beam divergence (0.3 mrad) and the maximum target distance (200m) are comparably low, whereas target objects on apron surfaces are rather large compared to other laser object detection applications (e.g. wrench, suitcase).

provided to the object detection/segmentation algorithm for offline processing. TABLE 1 indicates, whether an object could be detected or not. If an object was detected in both poses (or could not be detected in any pose), no distinction was made in the respective column in TABLE 1.

TABLE 1. Detectability over distance for all objects

Detect-ability over Distance	**Object A** Standard. 1 m2	**Object B** Standard. 0.063 m2	**Object C** Standard. 0.0006 m2	**Object D** Real Suitcase Pose: 1 | 2	**Object E** Real Toolbox Pose: 1 | 2	**Object F** Real Wrench Pose: 1 | 2
25m	✓	✓	×	✓	✓	✓
60m	✓	✓	×	✓	×/✓	×
95m	✓	✓	×	✓	×	×
130m	n.a.	n.a.	n.a.	n.a.	n.a.	n.a.
165m	✓	✓	×	✓	×	×
200m	✓	✓	×	×	×	×

TABLE 1 clearly shows that two of the *standardized objects* (object A and B) were detected over the entire range of distances. This indicates a strong influence of the target`s reflectivity coefficient ρ (surface material, beam angle of incident), which was intentionally kept high for the standardized objects by using retroreflectors (see section 4.3). From the algorithm perspective, however, this applies only to objects larger than a critical minimal size, as the non-detectability of the extremely small object C demonstrates. This potential correlation between target size and detectability may also be assumed for the object D (suitcase). Since the reflection coefficient of the fabric material of a suitcase is substantially lower than that of a retroreflector, the reason why object D was successfully detected is the comparably large size of its effective target surface (successful detection over all distances except for 200m). Apparently, the two remaining *real objects* (object E and F) were not detected due to the extremely small size: Object E (toolbox) could only be detected up to a maximum range of 60m (only pose 2), and object F (wrench) was even more limited to 25m.

5.3 Time to Detection

The TTD (here: *acquisition time*) is determined by the number of captured points ($\#points_{min}$) necessarily required for the detection of a particular object. This is only possible for those object-distance relations that have been successfully detected before (refer to TABLE 1). In detail, the quantity $\#points_{min}$ is approximated by manually reducing the total number of measured reflection points ($\#points_{total}$), until a critical number of points was reached. Based on the quantity, the time span required for detection is read from the time stamps of the first and the last 3D point stored in the data file. TABLE 2 shows the results of the distance-related TTD for object A, pose 1 and for object D, pose 1, respectively. The total data acquisition time SAT_{total} gives rise to the $\#points_{total}$.

TABLE 2. TTD over distance for object A (standard, 1sqm) and object D (suitcase)

Distance	**Object A** Standard. 1 m2 **$\#points_{min}$**	**Object A** Standard. 1 m2 **TTD [s]**	**Object D** Real Suitcase Pose: 1 **$\#points_{min}$**	**Object D** Real Suitcase Pose: 1 **TTD [s]**
25m	50000	0,6	100000	1,2
60m	500000	5,9	2000000	23,5
95m	1000000	11,8	3000000	35,3
130m	n.a.	n.a.	n.a.	n.a.
165m	2000000	23,5	5000000	58,8
200m	4000000	47,1	not detected	n.a.

In Figure 11 we plot the TTD of all objects (pose 1) as a function of their distances from the scanner. According to TABLE 2, the TTD for both object E (toolbox) and F (wrench) could only be determined for a value of 25m.

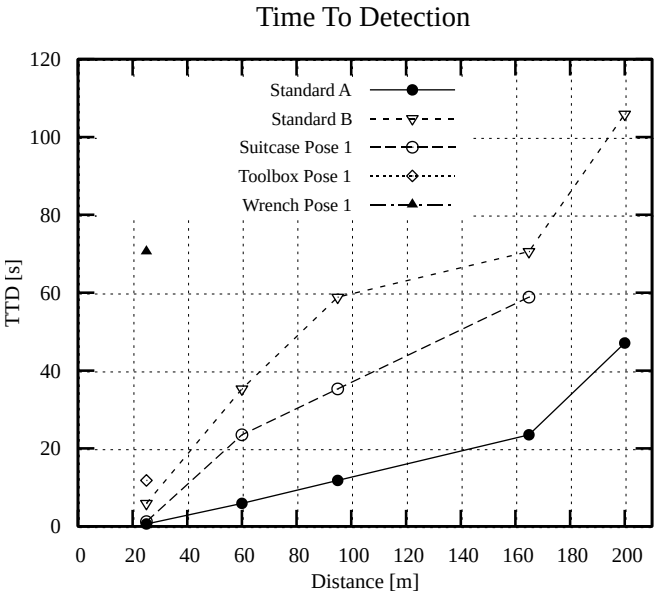

Figure 11. TTD over distance for all objects

As the diagram in Figure 11 is based on a single dependent variable (TTD) and a single independent variable (distance), a linear regression analysis was applied to determine whether a linear correlation exists in the data. The results for object A, B and D can be found in TABLE 3:

TABLE 3. Linear regression between TTD and distance

Object	**Coefficient of determination R^2 [%]**	**p-value [%]**
Object A Standard.	90.4	0.01291
Object B Standard.	83	0.03149
Object D Suitcase	97	0.01304

From the coefficients of determination R^2, which are all 83% and higher, and the low p-values, linearity between distance and detectability seems very likely. This linearity might be explained from the geometrical relationship between the detection performance and the sensor-target distance. Assuming that the detection of a target object corresponds to a certain *minimum number of pulses reaching the target`s surface* (n_{min}), the

geometric relation between the number of these pulses and the distance between sensor and target may be modelled as follows:

Let ρ denote a *number of pulses emitted in a certain time by the sensor*, the direction of propagation of these pulses can be probabilistically regarded as uniformly distributed on a 2D unit sphere with a total surface size (A_{total}). This assumption is based on the earlier introduced sensor scan pattern and the sensor`s static field of view, which is defined by its aperture angles. Therein, the spherical surface (A') represents the projection of the *effective reflective area of the target object* (*A)* over a *distance* (*r)* on the unit sphere. This may be described by the following simple projection relation:

$$A/r \approx A' \qquad (3)$$

where $r \gg 1$ (refer to Figure 12). Consequently, the *number of pulses reaching the target`s surface* (*n)* is a subset of the total number of pulses, described as a function of *time* (*t)*:

$$n = \rho \cdot t \cdot A'/A_{total} \qquad (4)$$

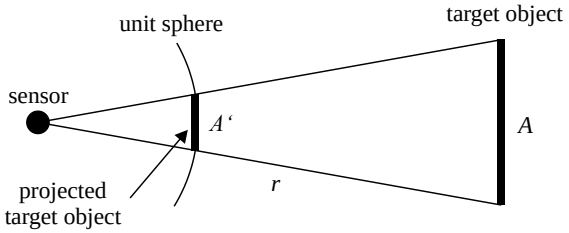

Figure 12. Projection model of the reflective surface of the target object

Referring to this projection function, the *minimum time* t_{min} for detecting a target object may be modelled as a function of the distance *r*:

$$t_{min} = \frac{n_{min} \cdot A_{total} \cdot r}{\rho \cdot A} \qquad (5)$$

Based on equation (5), linearity between distance and detectability can be confirmed. This particular finding and the theoretical assumptions from section 3.2, equation (2) (inverse proportionality between $P_{R\_hard\ target}$ and the squared distance), lead to a major discrepancy. This discrepancy may be explained by the working principle of our detection/segmentation algorithm not covered in the theoretical considerations on the signal level. Furthermore it shall be noted that ideal reflection conditions in terms of the target surface`s reflection coefficient and the beam angle of incident are passed as input into the model depicted in Figure 12. However, up to a certain degree these properties may be assumed for the *standardized objects* used in this field study. Atmospheric transmission effects, which were comparably constant over the entire measurements, may be also neglected in this approximate analysis.

6. CONCLUSION & OUTLOOK

In this paper, the combined detection performance of the tested LiDAR system consisting of the sensor itself and the detection/segmentation algorithm was demonstrated and quantified for six test objects, using the performance metrics *Detectability* and *Time To Detection* (TTD). The results are promising for the large and mid-size *standardized objects*, as well as for *real objects* of comparable size (e.g. the suitcase). It turns out that the size of the target`s reflection area and its reflection properties are key factors for detection. Interestingly, with increasing distances the reflection properties seem to be more important than size (the retroreflector Object B is about half of the size of Object D (suitcase), but was detected at a distance of 200m, whereas Object D was not). In summary, we see our detection/segmentation techniques as a sound basis for higher level recognition tasks, such as object classification and tracking of comparably large aircraft and vehicles.

Furthermore, we found linearity between distance and detectability. This fact, however, needs further investigation since the theoretical considerations on signal level (section 3.2) rather suggest a squared relationship. The results of this investigation will become relevant for identifying optimized sensor positions in terms of the safety-effective surveillance of an apron area.

In the scope of our ongoing overall risk assessment described in section 2.1, the feasibility to address an exemplary, but nevertheless important hazard was demonstrated on the example of FOD. The following observations were made: Assuming an FOD scenario, where a suitcase is lost on the apron, our current LiDAR system requires at most 60s to detect FOD within a radius of 165m around the sensor (see TABLE 2). Once detected, the information will be visually forwarded to the apron controller in accordance to our surveillance concept. From the above example (suitcase, distance 165m, TTD 60s) it follows that the automatic FOD detection system covers a circular area of about 85530 m2/ 8.5 hectare around the sensor (given that the sensor is positioned in the center of a dedicated apron area without occlusion). A system that is capable to comprehensively cover and methodically scan a defined apron area stands in contrast to today`s procedures for FOD detection, which rely on random observations from apron personnel and on inspections. Even though these inspections are carried out on a regular base, they are too sparse and, in the most cases, they are limited to the runway system.

From the perspective of the current detection and segmentation schema, we see at least two directions for performance improvements. Regarding the detection of extremely small objects (like Object C, E and F), firstly we believe that the additional utilization of the return-beam power ratio value stored for each reflection point will significantly contribute to the detection performance. In a first manual analysis involving these values, we could visually confirm the positions of object C and object F in a distance of 200m. Secondly, to better distinguish extremely small objects from the background it is immanent to derive highly discriminative object class specific features and/or appearance attributes. For example, a distinction between foreground- and background-objects may readily be derived from the fact that different types of surfaces give rise to different return-beam power ratios of the scanned 3-D points. In our preliminary experiments we were able to increase the speed of the foreground-background segmentation algorithm by a factor of 4.

In order to detect and segment object candidates in real-time (*computing times < acquisition time*) both the feature extraction and the fg-bg segmentation must be in line with the data acquisition, which means that the processing is done continuously on the acquired data stream. From this is follows that certain features which may seem useful (e.g., collecting statistics on all neighboring points within a bounded region) may not be feasible.

All of the above improvements regarding static object detection will be tested within a second field trial at Dresden airport scheduled for autumn 2015. To prove LiDAR`s prospected high

degree of independency against view-restricting weather and lighting conditions, this field trial will also be conducted under various adverse weather conditions (e.g. heavy rain, fog).

Besides static object detection, the detection of moving objects will be another significant step forward in our research. This is, however, a major challenge, as typical apron taxing speeds can reach up to comparably high speeds in radial or tangential direction (10m/s). In parallel, object classification and tracking algorithms are under development to work towards the realization of the presented surveillance concept.

ACKNOWLEDGMENT

Our thanks go to Dresden airport for their extraordinary willingness to support our research throughout the whole project duration. We also thank Neptec Technologies for their support.

REFERENCES

[1] L. Meyer, J. Mund, B. Marek und H. Fricke, „Performance test of LiDAR point cloud data for the support of apron control services," in *Proceedings of the International Symposium on Enhanced Solutions for Aircraft and Vehicle Surveillance Applications (ESAVS)*, Berlin, Germany, 2013.

[2] J. Mund, L. Meyer und H. Fricke, „LiDAR Performance Requirements and Optimized Sensor Positioning for Point Cloud-based," in *Proceedings of the 6th International Conference on Research in Air Transportation*, Istanbul, Turkey, 2014.

[3] T. Horberry, M. A. Regan und S. R. Toukhsati, „Airport ramp safety and intelligent transport systems," *IET Itelligent Transport Systems*, pp. 234-240, 12 2007.

[4] C. Niessen und K. Eyferth, „A model of the air traffic controller`s picture," *Safety Science* , pp. 187-202, 2001.

[5] Australian Transport Safety Bureau, „Ground operations occurances at Australian airports 1998 to 2008," Canberra, 2010.

[6] Health and Safety Executive, „Aircraft turnround," Sudbury, 2000.

[7] Boeing, „Statistical Summary of Commercial Jet Airplane Accidents. Worldwide Operations 1959-2011," 2012 .

[8] A. B. E. Koustana, P. Elslande und C. Bastien, „Statistical analysis of "looked-but-failed-to-see" accidents," *Accident Analysis & Prevention*, Bd. 40, Nr. 2, pp. 461-469, 2008.

[9] International Civil Aviation Organization (ICAO), „Advanced Surface Movement Guidance and Control Systems (A-SMGCS) Manual. Doc 9830," ICAO, Montral, 2004.

[10] F. v. Hundelshausen, M. Himmelsbach, F. Hecker, A. Mueller und H.-J. Wuensche, „Driving with tentacles: Integral structures for sensing and motion," *Journal of Field Robotics - Special Issue on the 2007 DARPA Urban Challange*, pp. 640-673, 2008.

[11] T. Nothdurft, P. Hecker, S. Ohl, F. Saust, M. Maurer, A. Reschka und J. Böhmer, „Stadpilot: First fully autonomous test drives in urban traffic," in *14th International IEEE Annual Conference on Intelligent Transportation Systems*, Washington D.C, 2011.

[12] P. Steinemann, J. Klappstein, J. Dickmann, H.-J. Wünsche und F. Hundelshausen, „3D Outline Contours of Vehicles in 3D-LIDAR Measurements for Tracking extended Targets," in *Intelligent Vehicle Symposium* , Alcala de Henares, Spain, 2012.

[13] M.-O. Löwer, A. Sasse und P. Hecker, „Needs and potential of 3D-city information and sensor fusion technologies for vehicle positioning in urban environments," in *International Workshop on 3D Geo-Information* , Belgium , 2009.

[14] Federal Aviation Administration, „FAA needs to improve ASDE-X management controls to address cost growth, scheduled delays, and safety risks," Washington , 2007.

[15] G. Galati, „Advanced integrated architecture for airport ground movements surveillance," in *Radar Conference*, 1995.

[16] M. Ferri, G. Galati, A. De Fazio und P. Magaro, „Milimetre-wave radar applications in airports: experimental results," in *First European Radarn Conference* , 2004.

[17] SESAR Consortium, „The ATM Target Concept D3," SESAR Consortium, Brussels, 2007.

[18] B. Zhang, W. Smith und S. Walker, „3-D Object recognition from point clouds," in *Proceesdings from ILMF*, 2011.

[19] A. Friedrich, "Evaluierung von Methoden zum Erstellen und Aktualisieren von sicherheitskritischen Flughafendatenbanken nach RTCA Do-272a, TU Darmstadt, 2008.

[20] R. Rasshofer und K. Gressner, „Automotive radar and lidar systems for next generation driver assistance functions," *ARS*, pp. 205-209, 2005.

[21] E. Hollnagel, The ETTO Principle: EfficiencyThoroughness Trade-Off, Ashgate, 2009.

[22] L. Meyer und H. Fricke, „Functional Hazard Analysis of Virtual Control Towers," in *Procdgs of 11th IFAC*, Valencienne,FR, 2010.

[23] Federal Aviation Administration, „Avisory Circular 150/5210-24," 2010.

[24] Eurocontrol, „Information Paper on French Study on Automatic FOD Detection Systems - Workshop Eurocontrol," Brussels, 2008.

[25] Bureau d'Enquêtes et d'Analyses pour la sécurité de l'Aviation civile, „Accident on 25 July 2000 to the Concorde. Final Report," Le Bourget, 2002.

[26] National Aerospace FOD Prevention, Inc., „National Aerospace FOD Prevention, Inc.," [Online]. Available: http://www.nafpi.com.

[27] I. McCreary, „Runway Safety: FOD, Birds, and the Case for Automated Scanning," *Insight SRI*, pp. 146-157, 2010.

[28] International Civil Aviation Organization (ICAO), „Annex 14 - Volume I Aerodrome Design and Operations," ICAO, Montreal, CA, 2009.

[29] P. Beasley, G. Binns, R. Hodges und R. Badley, „Tarsier, a millimetre wave radar for airport runway debris detection," in *EURAD Radar Conference*, 2004.

[30] M. Endsley, „Design and Evaluation for Situation Awareness," 1988.

[31] M. Endsley, „Toward a Theory of Situation Awareness in Dynamic Systems," *HUMAN FACTORS*, pp. 32-64, 1995.

[32] D. Jones und M. R. Endsley, „Sources of situation awareness errors in aviation," *Aviat Space Environ Med.*, 1996.

[33] M. Hebel, M. Arens und U. Stilla, „Change detection in urban areas by object-based analysis and on-the-fly comparison of multi-view ALS data," *ISPRS Journal of Photgametry and Remote Sensing*, pp. 52-64, 2013.

[34] Y. Boykov und K. V., „An Experimental Comparison of Min-Cut/Max-Flow Algorithms for Energy Minimization in Vision," in *PAMI* , 2004.

[35] U. Wandinger, „Introduction to Lidar," in *Lidar - Range-Resolved Optical Remote Sensing of the Atmosphere*, New York, Springer , 2005, pp. 1-18.

[36] R. Measures, Laser Remote Sensing: Fundamentals and Applications, New York: Wiley-Interscience, 1984, p. 521.

[37] J. Ludwig, „Bewertung von Sensorstandorten von LiDAR Überwachungstechnik für die optimale Objektdetektion auf dem Standplatz eines Flughafenvorfeldes," 2012. [Online]. Available: http://www.ifl.tu-dresden.de/?dir=Studium/Studien--Diplomarbeiten.

[38] Neptec Technologies , „OPAL-360 Sensor 2.0. User Manual," 2013.

[39] M. Endsley, Theoretical underpinnings of situation awareness: A critical review. In M.R. Endsley & D.J. Garland (Eds.), Mahwah, NY, 2000.

[40] ESARR SRC, „Eurocontrol safety regulatory requirement 4 - risk assess-ment and mitigation in ATM," Eurocontrol, Brussels, BE, 2001.

[41] J. Johnson, Analysis of Image Forming Systems, 1958.